Earth Planet. Sci. Lett. 641 (2024) 118831

Contents lists available at ScienceDirect

Earth and Planetary Science Letters

journal homepage: www.elsevier.com/locate/epsl

Changes of North Atlantic plate motion in early Paleogene driven by Icelandic plume: Insights from kinematic and stratigraphic constraints

Zhirui Ray Wang [a,*], Giampiero Iaffaldano [b], John R. Hopper [a,c]

[a] Department of Geosciences and Natural Resource Management, University of Copenhagen, Øster Voldgade 10, Copenhagen, 1350, Denmark
[b] Dipartimento di Scienze Chimiche, della Vita e della Sostenibilita Ambientale, Universita' di Parma, Via delle Scienze, 157/A, Parma, 43124, Italy
[c] Department of Geophysics and Sedimentary Basins, Geological Survey of Denmark and Greenland, Øster Voldgade 10, Copenhagen, 1350, Denmark

ARTICLE INFO

Editor: A. Webb

Keywords:
plate motion changes
dynamic topography
mantle convection
North Atlantic
Icelandic plume

ABSTRACT

Mantle convection is a fundamental process that shapes the Earth's surface by providing the driving and resisting forces for horizontal motion of tectonic plates, as well as for inducing non-isostatic vertical motion commonly termed "dynamic topography". Growing observational constraints of past plate motion and dynamic topography have led to better understanding of the history of surface expression induced by mantle flow. Often these two surface motion signals are studied separately. However, the existence of a thin, mechanically weak asthenosphere allows geodynamicists to link horizontal and vertical motion changes together via mantle flow properties in the context of pressure-driven Poiseuille-type flow. In this paper, we utilize publicly available geologic and geophysical datasets to study early Paleogene plate kinematics and spatiotemporal evolution of dynamic topography in the North Atlantic region. We find that the North America (NAM) and Greenland (GRN) plates experienced a rapid kinematic change around late Paleocene–early Eocene, coinciding with episodes of surface uplift inferred from stage-resolution stratigraphic information around the North Atlantic, Labrador Sea and Baffin Bay. We quantitatively tie these surface motion signals together to underlying asthenospheric flow processes by estimating torque variations on NAM and GRN. These are parameterized in terms of reconstructed kinematic changes as well as predicted Poiseuille-type flow induced by increasing Icelandic plume flux and speedup of Farallon slab. Our analysis indicates (1) that the torque-change associated with the Icelandic plume flux closely resembles the ones inferred from kinematic reconstructions, and (2) that the inclusion of slab effects does not modify significantly such a scenario. Our findings shed light on the role of asthenospheric channelized flow generated by the Icelandic plume in influencing the early Paleogene North Atlantic surface dynamics.

1. Introduction

Mantle convection is a fundamental process of the Earth system, as it serves the purpose of releasing heat and manifests itself at the surface over geologic time (Davies and Richards, 1992). It provides driving and resisting forces for the motions of tectonic plates (e.g., Hager and O'Connell, 1981), the history of which has been reconstructed from progressively-denser sampling of ocean-floor magnetization (e.g., Seton et al., 2014). These reconstructions provide information of relative motions between any two neighboring spreading oceanic plates (e.g., Chase, 1978; Minster and Jordan, 1978). Such relative plate-motion pairs, moreover, can be combined to form plate circuits, which helps to explore global kinematic patterns (e.g., Müller et al., 2016). In spherical geometry and under the approximation of plate rigidity (Gordon, 1998), the inferred plate motions can be expressed via Euler vectors (e.g., Morgan, 1968; McKenzie and Parker, 1967). The latter are often accompanied by uncertainties that can be expressed in the form of covariance matrices (Chang et al., 1990). To date, reconstructions of past plate motions have reached an impressive level of sophistication for both regional (e.g., Gaina et al., 2002, 2009, 2017; Causer et al., 2021) and global (e.g., Müller et al., 2016) domains, particularly for motions during the Cenozoic era. These reconstructions reveal that plate kinematic changes of up to 20-30% occur rapidly, that is, within intervals of few Myrs (e.g., Iaffaldano and Bunge, 2015).

In this context, it is well known that the presence of a thin, low-viscosity sublithospheric layer (the asthenosphere) plays a critical role in Earth's mantle convection (see Richards and Lenardic (2018) for a review). The mechanical weakness of the asthenosphere allows the

* Corresponding author.
E-mail address: zhirui@ign.ku.dk (Z.R. Wang).

https://doi.org/10.1016/j.epsl.2024.118831
Received 1 November 2023; Received in revised form 20 May 2024; Accepted 2 June 2024
Available online 12 June 2024

emergence of channelized fast flow (e.g., Höink and Lenardic, 2008, 2010), which in turn modulates the large-scale convective planform (e.g., Bunge et al., 1996). Importantly, such flow features both Couette and Poiseuille components. The former is driven by moving tectonic plates, while the latter is driven by lateral pressure gradients (e.g., Stotz et al., 2018). The notion that both components are additive and contribute independently to the channelized flow, evidenced by the linear independence of associated terms within the dynamic-balance equation (e.g., Davies, 1999), is important to recognise: the relative partitioning of Couette and Poiseuille flow determines whether stresses at the base of lithosphere are in accord with, or against, plate motions, that is, whether a tectonic plate drives or resists the asthenospheric flow beneath (Iaffaldano and Bunge, 2015). Early studies proposed that the Poiseuille flow can be induced by rising mantle plumes, as hot upwelling provides asthenospheric influx, and generates lateral pressure variations (e.g., Phipps Morgan et al., 1995). Furthermore, a range of computer simulations of mantle flow suggests that lateral pressure gradients may form in an internally-heated convection system (Höink and Lenardic, 2008, 2010). This result means that asthenospheric Poiseuille-type flow can also be induced by cold downwellings associated with sinking subducted slabs, in the absence of plumes.

The notion that asthenospheric Poiseuille-type flow is an integral part of mantle convection facilitates relating lateral pressure gradients to mantle-flow induced surface topography. In fact, the latter one, referred to as “dynamic topography” (Hager et al., 1985), can be studied as an expression of pressure distribution within the asthenosphere. Contrary to the plate kinematic history, which has been investigated and reconstructed extensively, inferences of past dynamic topography have remained mostly sparse (see Hoggard et al. (2021) for a review). In recent years, this topic has received renewed attention, owing to the fact that the transient nature of dynamic topography leaves imprints in the sedimentary record (e.g., Mitrovica et al., 1989; White and Lovell, 1997; Friedrich et al., 2018). Such an approach has been applied for the first time in regions that experienced low dynamic topography, like the Cretaceous Interior Seaway of North America, where extensive platform subsidence generated sufficient space to retain sediments (e.g., Mitrovica et al., 1989). Efforts dedicated for inferring past dynamic-topography highs have also been made in offshore areas, for instance near the British Isles, where pulses of sub-marine fan deposition are interpreted as a proxy for episodic uplifts of neighboring lands (e.g., Jones et al., 2001, 2002; White and Lovell, 1997). These inferred dynamic uplifts, importantly, provide strong evidence for the existence of the Icelandic plume. The latter has been extensively investigated in terms of its past activity and associated surface expressions based upon studies of V-shaped ridges (e.g., Davis et al., 2012; Parnell-Turner et al., 2014, 2017; White, 1997) and deep-water currents (e.g., Parnell-Turner et al., 2015; Poore et al., 2006) in the North Atlantic region. Recently, Friedrich et al. (2018) proposed a novel technique that interprets inter-regional scale unconformities seen in geologic maps as the records of sedimentary hiatus: a missing period in the rock record (Miall, 2016). Hiatuses potentially reveal continental-scale erosion/non-deposition environments, and thus are interpreted as a result of past dynamic uplift. This method has been applied in order to map the spatio-temporal evolution of hiatus/deposition in individual (e.g., Brown et al., 2022; Vibe et al., 2018) and multiple (Hayek et al., 2020) continents since the Upper Jurassic. These maps evidence how, over geologic time, the distribution of hiatus/deposition environments may vary significantly across and between continents. The spatial extent of hiatuses, moreover, can reach up to ∼5000 km, a length consistent with the range of wavelengths of dynamic-topography signals induced by upper-mantle heterogeneity (Richards et al., 2020).

The histories of horizontal plate motions on the one side, and vertical lithospheric uplift/subsidence on the other are traditionally studied separately. However, the theoretical framework associated with asthenospheric Poiseuille flow provides a way to link these histories and tie them to the characteristics of the underlying mantle flow. Colli et al. (2014) used a plate torque-balance estimates to show that pressure-driven flow is capable of generating sufficient basal shear to drive the past motion of the South American plate. Furthermore, they found that changes in spreading velocity of the South Atlantic Ridge correlate with changes in the geologically-constrained vertical motions of the surrounding continents. Vilacís et al. (2022) noted this correlation occurred frequently in the Atlantic and Indo-Australia regions, where a change in spreading rate is often followed by a change in topography of the surroundings, inferred from continental-scale hiatus maps. Vilacís et al. (2022) also employed an analytical model to mimic the first-degree Poiseuille flow field generated by a plume. They showed that the extent of the region featuring significant Poiseuille flow underneath (at the peak of the model hotspot activity) was comparable to that of the region exhibiting a hiatus, suggesting that upwelling plume activity can be responsible for plate motion changes. Wang et al. (2023) extended the asthenospheric flow model by incorporating the effect of sinking slabs. The latter reveals a source-to-sink relation, in which the asthenospheric material sourced from plumes is driven towards subducted slabs. They found that inclusion of slabs promotes the long-range transport of warm, buoyant mantle material injected by plumes, and modulates the basal shear stress acting upon plates. These findings suggest exploring further the possible role of asthenospheric channelized flow, generated by a combination of plume and slab effects, in causing temporal variations of surface plate motions.

There are two reasons why the North Atlantic region is an ideal candidate to evaluate the relationship between its plate-motion history and the underlying asthenospheric flow: (1) it holds abundant geophysical and geological observations, including extensive coverage of ocean-floor magnetization measurements (e.g., Gaina et al., 2002, 2009, 2017; Causer et al., 2021), and well-documented stratigraphic record in both onshore and offshore regions (e.g., Hopper et al., 2014; Gregersen et al., 2019). The former helps to infer the North Atlantic plate kinematic history, thus providing direct constraints on the force-balance of tectonic plates (e.g., Iaffaldano and Bunge, 2015). The stratigraphic record can be used to interpret the spatio-temporal evolution of past dynamic-topography signals in the form of hiatus maps. Importantly, the North Atlantic stratigraphic dataset is compiled at a temporal resolution similar to geologic stages (∼1-5 Myrs), and thus finer than that of geologic series (∼10-20 Myrs) utilized in previous inferences (e.g., Hayek et al., 2020). Such finer resolution introduces the possibility of deducing the North Atlantic vertical motion history in greater detail. (2) Inferences from seismic tomography studies (e.g., Celli et al., 2021) and buoyancy flux estimates (e.g., Hoggard et al., 2020; Ribe et al., 2020; Parnell-Turner et al., 2017) evidence the presence of a deep seated mantle plume beneath Iceland. The latter has profoundly influenced the North Atlantic surface expression (e.g., Anell et al., 2009; Dam et al., 1998; Jones et al., 2002) and underlying asthenospheric flow properties (e.g. Hartley et al., 2011; Rudge et al., 2008). Furthermore, the channelized flow induced in the asthenosphere by the Icelandic plume may be further modulated by the Poiseuille-type flow generated by the descent of the Farallon slab, through the mechanism described above.

In this study we aim at disentangling the role of asthenopsheric flow components in affecting the early Cenozoic surface motions of the North Atlantic and surrounding plates. We focus on the late Paleocene–early Eocene period, as it coincides with a major phase of Icelandic plume activity inferred from studies of mantle temperature fluctuation in V-shaped ridges (e.g., Parnell-Turner et al., 2014), magmatic productivity in adjacent conjugate margins (e.g., Holbrook et al., 2001), and widespread appearance of the flood basalts (e.g., Wilkinson et al., 2017). We start by investigating the North Atlantic plate kinematic history, utilizing publicly available finite rotations. We proceed by resorting to a recently-compiled stratigraphic dataset to infer the past dynamic topography at a temporal resolution of geologic stages. Next, we quantitatively link the two categories of observations by modeling the North Atlantic asthenospheric flow. The latter is parameterized as superimposition of Poiseuille-type flow terms associated with (1) in-

creased Icelandic plume flux, and (2) speedup of Faralon slab. We then use the asthenospheric flow prediction to calculate torque variations upon plates, and compare these with the ones required in order to explain changes in the North Atlantic plate motions. Lastly, we discuss uncertainties and implications associated with the observations and modelling strategy utilized.

2. Reconstructed late Paleocene-Eocene plate kinematics

We investigate late Paleocene-Eocene plate kinematics of the North Atlantic region by examining two relative plate motions: (1) North America relative to Eurasia (NAM/EUA) based on Causer et al. (2021), and (2) Greenland relative to Eurasia (GRN/EUA) based on Gaina et al. (2017). We choose EUA as a fixed reference frame, as it has the largest basal area among the tectonic plates in the region. This inference implies that EUA would require a larger torque to modify its motion, due to the larger viscous resistance exerted at the base of lithosphere by the asthenosphere underneath. Therefore, of all plates in the region, EUA is arguably the least likely to change its motion through time in a way detectable via ocean-floor magnetisation, given the same torque variation. For NAM/EUA, we utilize the finite rotation dataset of Causer et al. (2021), which is built upon the previous compilation by Gaina et al. (2002). Importantly, the NAM/EUA finite rotations from Causer et al. (2021) exclude the magnetic isochron picks in the Greenland-Lofoten Basins. Exclusion of these magnetic picks ensures that the effects of the Jan-Mayen micro-continent formation are not propagated to the analyses, and misinterpreted as changes of NAM/EUA motion. For GRN/EUA, we use a recent compilation from Gaina et al. (2017), which is based on an augmented dataset of magnetic-anomaly picks and fracture zone identifications relative to their previous work (Gaina et al., 2002, 2009).

We assign ages to each finite rotation according to the recently-updated geomagnetic polarity timescale of Ogg (2020). This procedure allows us to obtain a consistent, temporally-harmonized set of finite rotations across different data sources. We note that Gaina et al. (2017) do not contain information on covariances for uncertainty assessment. Therefore, we take a simple approach and assume that covariance matrices are diagonal. Next, we assign to each diagonal element a value equal to the trace computed from covariances of the temporally-closest finite rotation in Gaina et al. (2002). This approximation is based upon the fact that both studies have used broadly identical magnetic isochron picks and fracture zones to infer their finite rotations. This information makes us presume that covariances of the two datasets are somewhat similar. We also note that covariances from Causer et al. (2021) are provided in the spherical reference system (i.e., longitude, latitude, rotational angle). Here we convert these covariances to the Euler-angles domain: we first generate 10^6 randomly sampled finite rotations, then transform each sample of the ensemble into the Euler-angles reference system and compute associated covariances accordingly.

Fig. 1 summarizes the reconstructed plate kinematic history of the North Atlantic region during the Paleocene–Eocene. Figs. 1 a & c shows the NAM/EUA (panel a) and GRN/EUA (panel c) angular velocity (solid lines) and associated 68% confidence limits (hatched/faded areas). Overall a speedup of angular velocity ranging from ~0.3-0.4°/Myr is observed in both records around the late Paleocene–early Eocene. The onset of the NAM/EUA speedup occurs at ~57 Ma, followed by a more prominent speedup of ~0.2°/Myr around 53 Ma. The GRN/EUA speedup occurs at ~53 Ma, with another significant speedup of ~0.3°/Myr around 50 Ma. Figs. 1 b & d illustrate the temporal path of the associated Euler stage poles. Overall, poles are located near the present-day South Atlantic and South Africa realms, thus indicating a primarily westward motion for NAM and GRN relative to a fixed EUA.

To further investigate the identified late Paleocene–early Eocene speedup, we use Euler vectors to compute the stage surface velocities of NAM and GRN during late Paleocene–early Eocene, and assess from these the plate kinematic changes occurred through time. Table 1 displays the velocity stages used in our estimate, which correspond to geologic times before and after the changes discussed above for Fig. 1. Fig. 2 illustrates the results. NAM experienced a southwestward velocity change of ~2 cm/yr (Fig. 2a) relative to fixed EUA. Conversely, GRN experienced a northwestward velocity change of ~3 cm/yr (Fig. 2b).

Table 1
Velocity stages used in this study to infer late Paleocene-early Eocene plate kinematic change of the North Atlantic region. Ages are according to the recently-updated geomagnetic polarity timescale of Ogg (2020).

	Old stage [Ma]	Young stage [Ma]	Reference
NAM/EUA	53.250–57.101	48.878–53.250	Causer et al. (2021)
GRN/EUA	52.930–57.101	47.760–49.666	Gaina et al. (2017)

3. North Atlantic vertical motion history inferred from stratigraphic record

In previous studies, the notion of asthenospheric Poiseuille-type flow has been utilized to link rapid plate motion variations to dynamic topography induced by mantle flow (e.g., Vilacís et al., 2022; Colli et al., 2014; Stotz et al., 2018). In order to probe the Cenozoic vertical motion history of the North Atlantic region, we resort to publicly available stratigraphic range charts from the *Tectonostratigraphic Atlas of the Northeast Atlantic Region* (NAG-TEC) (Hopper et al., 2014), as well as to a recent compilation for West Greenland (Gregersen et al., 2019). These charts consist of mostly borehole (offshore) and outcrop (onshore) data. From these, we map associated stratigraphic columns in a temporal resolution of geologic stages (i.e., few Myrs). This resolution is finer than geologic series, which lasts ten Myrs to few tens of Myrs, used in previous studies (e.g., Hayek et al., 2020; Vibe et al., 2018). We follow the approach developed by Friedrich et al. (2018) and introduce two further refinements: (1) If a hiatus is present for several consecutive stages, we mark the last hiatus stage as “end of hiatus” and remaining as “ongoing hiatus”. The purpose of this distinction is to provide a degree of confidence in interpreting the hiatus signal, because deposition that occurred in a geologic stage might have been eroded in subsequent periods. In other words, “ongoing hiatus”/“end of hiatus” indicate a lower/higher degree of confidence in the inference that erosion and non-deposition happen in a geologic stage. (2) We incorporate sediment types recorded in stratigraphic columns by dividing “no-hiatus” into “terrestrial”, “marine” and “volcanic”. This categorization is useful in offshore regions, where an influx of terrestrial deposits can be treated as a further proxy for topographic uplift in surrounding lands (e.g., White and Lovell, 1997). Stratigraphic columns based on borehole data, which contains exact geographical coordinates, are marked as dots, whereas columns inferred from geologic outcrops are marked as diamonds. We also resort to a published geochrononlogical dataset of the North Atlantic Igneous Province (NAIP) (Wilkinson et al., 2017) in order to include additional extrusive volcanic deposits, and mark these as triangles.

Fig. 3 shows the compiled geological hiatus maps in the North Atlantic region from stages of **Danian** (66.0-61.6 Ma) to **Ypresian** (56.0-47.8 Ma), where ages are assigned to the updated chronostratigraphic timescale (Cohen et al., 2013). These geologic stages cover the Paleocene and early Eocene periods. They coincide with a major phase of Icelandic plume activity inferred from studies of mantle temperature fluctuation (e.g., Parnell-Turner et al., 2014) and magmatic productivity (e.g., Holbrook et al., 2001) in the North Atlantic region. For each stage, present-day coastlines and mapped features are reconstructed to their paleo-position using the global plate motion model of Müller et al. (2016). In the following, we summarize key stratigraphic features inferred for each stage: In the **Danian** (66.0-61.6 Ma) (Fig. 3a), broad-scale terrestrial deposition occurs between the Norwegian and eastern Greenlandic margins, indicating a topographic uplift in surrounding on-

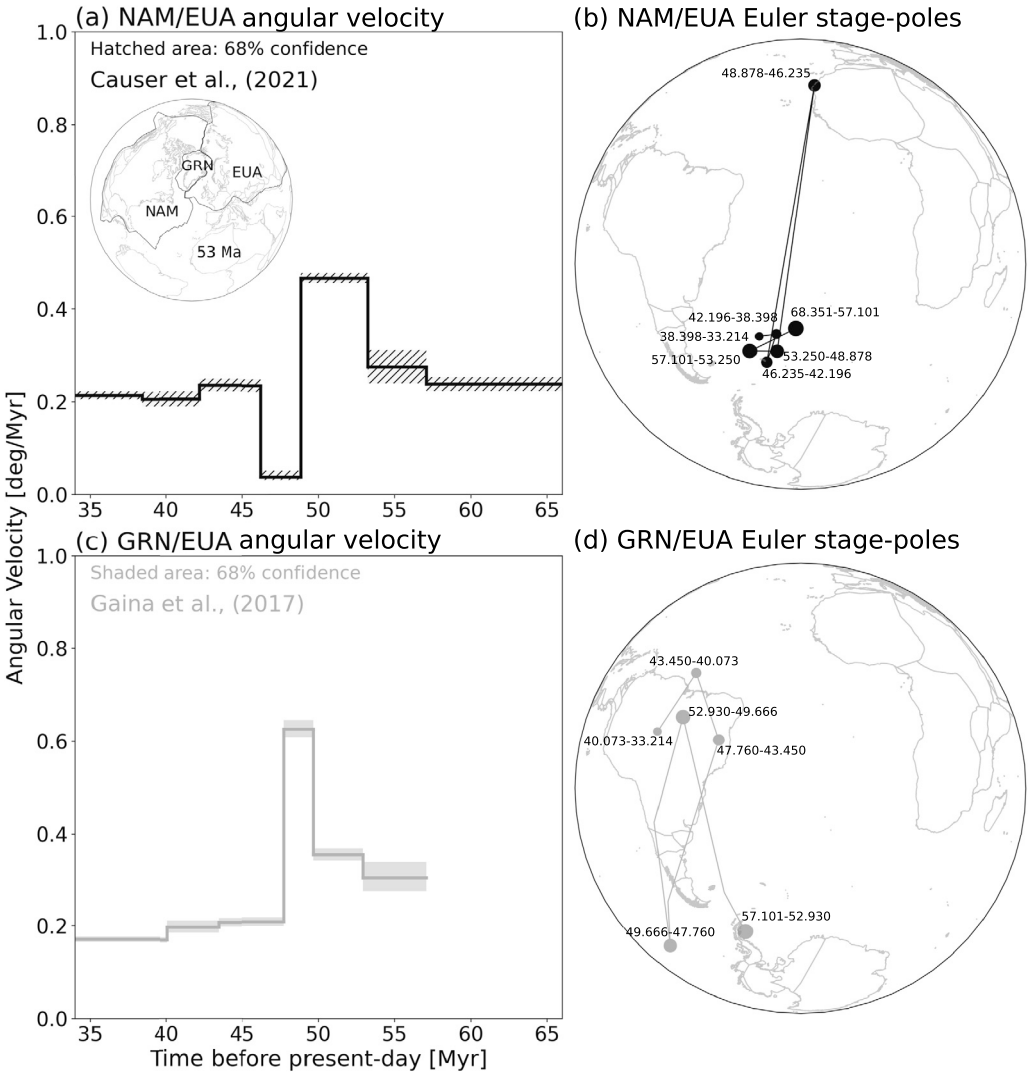

Fig. 1. Paleocene–Eocene (~66-34 Ma) plate kinematic history between North American/Eurasian plates (NAM/EUA; a-b) and Greenland/Eurasian plates (GRN/EUA; c-d), where EUA is fixed as a reference. a & c: Angular velocity under a temporal resolution of available stage rotations using a recently updated geomagnetic polarity timescale by Ogg (2020). Black and gray lines are based on Causer et al. (2021) and Gaina et al. (2017), respectively. Hatched and faded areas indicate 68% confidence interval. Both records show a speedup around late Paleocene–early Eocene (~57-53 Ma). Inserted globe depicts plate configuration at 53 Ma based on a plate reconstruction model (Müller et al., 2016). b & d: Associated stage Euler poles, in which marker size increases from the youngest to oldest stage. Numbers indicate their corresponding time period in the unit of Ma.

shore regions. An end-of-hiatus is seen near the southern part of West & East Greenland, indicative of a high topography with more confidence. An ongoing hiatus is observed in the northern portion of British Isles. In the **Selandian** (61.6-59.2 Ma) (Fig. 3b), marine sedimentation takes over the previous terrestrial deposits in the Norwegian Sea, and extends towards Svalbard, West Greenland and the Faroe-Shetland Basin, north of the British Isles. Together, these features suggest the lack of uplift activity during this period. In the **Thanetian** (59.2-56.0 Ma) (Fig. 3c), widespread volcanism appears near West and East Greenland, the Norwegian Sea, and west of the British Isles, contributing to the formation of NAIP (e.g., Wilkinson et al., 2017). Terrestrial deposition is clustered near southeastern Greenland, Svalbard, central Norwegian margin and Faroe-Shetland Basin, indicative of renewed uplifts. In the **Ypresian** (56.0-47.8 Ma) (Fig. 3d), marine sedimentation occurs near Svalbard and Norwegian margin, while volcanism continues in West & East Greenland and Faroe-Shetland Basin. On this basis, our inference is that the North Atlantic region underwent multiple uplift phases, prominently in **Danian** (66.0-61.6 Ma) and **Thanetian** (59.2-56.0 Ma), throughout Paleocene.

4. North Atlantic asthenospheric flow

Next, we turn our attention to assess the role of temporal changes of asthenospheric flow in modulating the North Atlantic surface expression in early Paleogene. To this end, one would generally need quantitative knowledge of the component of asthenospheric flow beneath tectonic plates that has, or is likely to have, changed over the time period covered by observations. Here we build a simple analytical Poiseuille-type model to estimate the asthenospheric flow field at mid-asthenosphere depth, and include effects owing to the rise of the Icelandic plume and/or the descent of the Farallon slab. First, in order to compute flow due to increasing Icelandic plume activity ($\Delta\bar{v}_{p,p}$), we adopt the approach of Iaffaldano et al. (2018); Vilacís et al. (2022), and approximate the rising plume as a point source that generates flux of material into the asthenosphere:

$$\Delta\bar{v}_{p,p}(\bar{r}) = \frac{H_a^2}{8\mu_a}\frac{\Delta P_p}{\Delta x}\cdot\hat{u}_p(\bar{r}) = \frac{H_a^2}{8\mu_a}\frac{\Delta\rho_{air}g\Delta h_p}{\Delta x}\cdot\hat{u}_p(\bar{r}) \quad (1)$$

where H_a is asthenospheric thickness, μ_a is asthenospheric viscosity, $\frac{\Delta P_p}{\Delta x}$ is plume-induced lateral pressure gradient within the astheno-

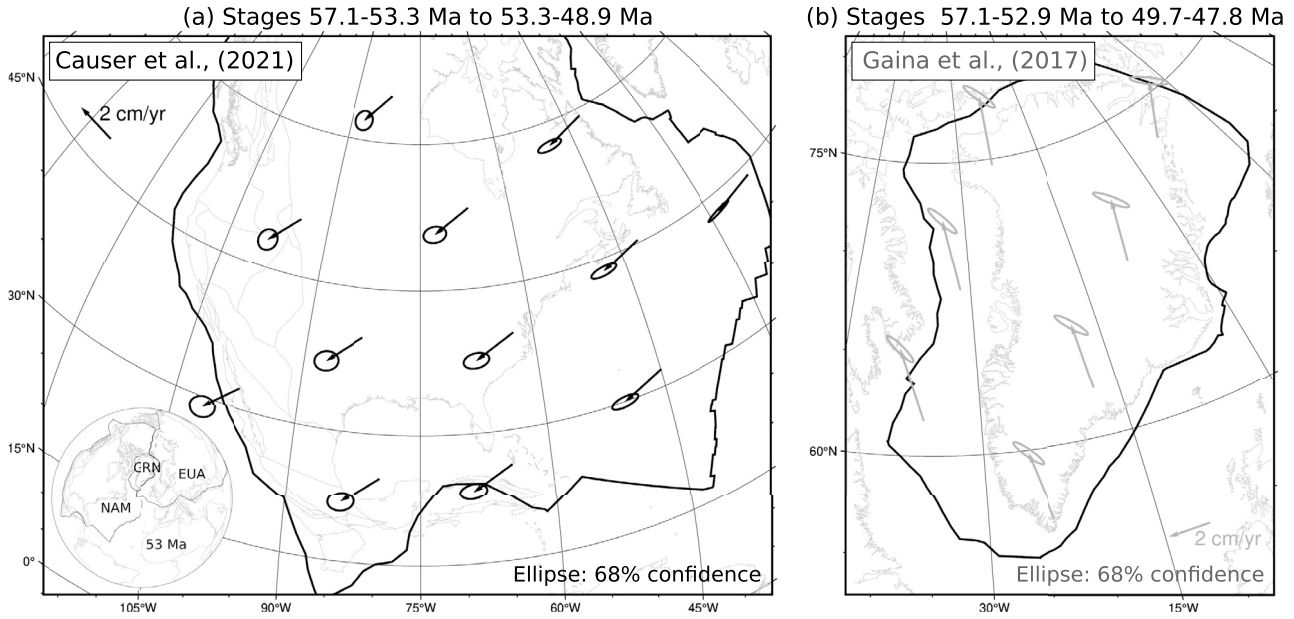

Fig. 2. (a): surface velocity change of NAM relative to fixed EUA in late Paleocene–early Eocene. (b): same as (a) but for GRN relative to fixed EUA. Overall, we note that NAM and GRN illustrate a divergent surface motion change relative to each other. Ellipse denotes 68% confidence. Exact ages of stages used are shown in Table 1. Present-day coastlines are reconstructed back to 53 Ma using a plate reconstruction model (Müller et al., 2016). Solid black line denotes associated plate contours, which are obtained from the same model above. Inserted globe depicts the North Atlantic plate configuration at 53 Ma.

Table 2
Notations used in this study.

Symbol	Description	Value	Units
$\bar{r}$	Position vector		
$\Delta\bar{v}_{p,p}(\bar{r})$	Change of plume flow velocity at $\bar{r}$		m/s
$\Delta\bar{v}_{p,s}(\bar{r})$	Change of slab flow velocity at $\bar{r}$		m/s
$\Delta P_p/\Delta x$	Plume induced lateral pressure gradient		Pa/m
$\Delta P_{s,i}/\Delta x_i$	Slab induced lateral pressure gradient		Pa/m
$\hat{u}_p(\bar{r})$	Unit vector for $\Delta\bar{v}_{p,p}(\bar{r})$		
$\hat{u}_i(\bar{r})$	Unit vector for $\Delta P_{s,i}/\Delta x_i$		
$\bar{v}'_{p,s}$	Prescribed slab flow velocity		m/s
$\bar{v}^0_{p,s}$	Slab flow velocity beneath subduction zone		m/s
H_a	Asthenospheric thickness		m
μ_a	Asthenospheric viscosity		Pa · s
$\Delta\rho_{air}$	Density contrast between mantle and displaced air	3300	kg/m^3
g	Gravitational acceleration	9.81	m/s^2
Δh_p	Dynamic-topography change due to plume		m
$\Delta\bar{M}$	Torque variation inferred from plate kinematics		N · m
$\Delta\bar{M}_p$	Torque variation predicted from analytical models		N · m
$\bar{v}$	Plate velocity		m/s
t_1	Time after plate-motion change		s
t_2	Time before plate-motion change		s
$\Delta\bar{\omega}$	Change of Euler vectors		rad/s
$\mathbf{C}$	Linear operator for torque analysis		
A	Plate basal area		m^2

sphere, Δx is geographical distance from the present-day location of Icelandic plume center, $\bar{r}$ is a generic geographical location at mid-asthenospheric depth, $\hat{u}_p(\bar{r})$ is a unit-vector field at position $\bar{r}$ (see Table 2). For the sake of simplicity, we assume a fixed plume location over time. ΔP_p can be estimated as $\Delta\rho_{air} g \Delta h_p$, where $\Delta\rho_{air}$ is the density contrast between mantle and displaced surface layer (i.e., air) due to dynamic topography high (3300 kg/m^3), g is the gravitational acceleration constant (9.8 m/s^2), and Δh_p is the dynamic-topography change owing to the Icelandic plume flux variation. We assign 700 m to Δh_p, as this value is consistent with inferences from paleo-landscape studies in the British Isles (e.g., Jones et al., 2002; Hartley et al., 2011). They have suggested the occurrence of a ~500–900 m transient uplift over a 1–3 Myrs interval in late Paleocene-early Eocene due to the passage of buoyant Icelandic plume material in the asthenosphere.

In order to estimate the Poiseuille-flow component induced by the descending Farallon slab, we approximate the latter as a line sink that draws surrounding asthenospheric material towards its location. The slab geometry is discretized as multiple point sinks, each of which produces a convergent (i.e., directed towards the sink location) Poiseuille-flow pattern. For the sake of simplicity, we assume that the slab descends vertically, and place the location of line sink at the paleo position of the Farallon/North America convergent boundary. The latter is determined following on the workflow developed by East et al. (2020). We then compute the total Poiseuille-flow component $\Delta\bar{v}_{p,s}(\bar{r})$ associated with the line of sinks at the generic geographical position $\bar{r}$ in

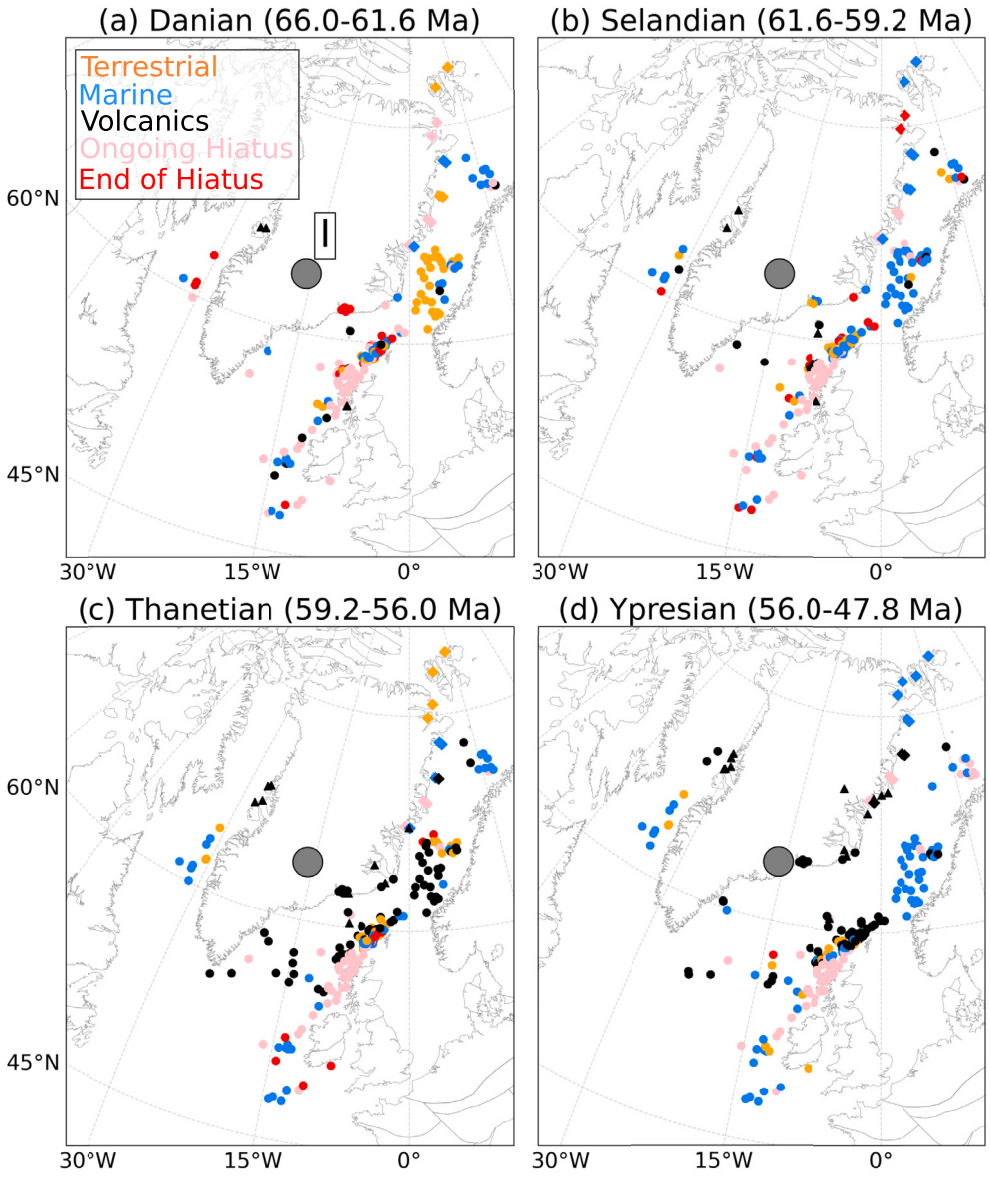

Fig. 3. Geological hiatus maps (GHMs) of the North Atlantic region with a temporal resolution of geological stages from the Danian datum to the Ypresian datum (a-d), where ages are assigned the updated chronostratigraphic timescale of Cohen et al. (2013). Each panel displays occurrence of terrestrial (orange), marine (light blue), volcanic (black) deposits, as well as ongoing hiatus (pink) and end of hiatus (red) in corresponding stage (see text for details). Dots and diamonds are inferred from ocean drilling and outcrop data, respectively, from a compiled stratigraphic-range chart dataset (Hopper et al. (2014)). Black triangles are based on a geochronological database of the North Atlantic Igneous Province (NAIP) (Wilkinson et al. (2017)). Grey circle indicates the present-day location of the Icelandic (I) plume Courtillot et al. (2003). Present-day coastlines are reconstructed with respect to a plate motion model tied to a global moving hotspot reference frame (Müller et al. (2016)). In the Danian, a regional-scale influx of terrestrial sediments was observed in offshore Norwegian and east Greenlandic margins, indicating a growth of topography in surrounding onshore regions. This terrestrial influx is followed by an increase of volcanic activities in succeeding stages.

mid-asthenosphere depth by taking the vector summation of individual point-sink fields:

$$\Delta\bar{v}_{p,s}(\bar{r}) = \sum_{i=1}^{n}\left(-\frac{H_a^2}{8\mu_a}\frac{\Delta P_{s,i}}{\Delta x_i}\right)\hat{u}_i(\bar{r}) \tag{2}$$

where i and n denote index and number of sinks, respectively, $\frac{\Delta P_{s,i}}{\Delta x_i}$ is the lateral pressure gradient associated with the point-sink, $\hat{u}_i(\bar{r})$ is a unit-vector field related to the i-th sink.

The study of Wang et al. (2023) has linked $\Delta P_{s,i}$ to slab induced dynamic subsidence. However, studies of the stratigraphic record (e.g., Mitrovica et al., 1989) and continental-scale hiatus maps (Hayek et al., 2020; Vilacís et al., 2022) have suggested a late Cretaceous-Tertiary rebound in the western interior of North America, immediately following its long-lasting low dynamic topography. In principle, this rebound would not produce a Poiseuille-type flow towards the subduction zone. Here we propose an alternative scenario where such flow can be generated by an absolute speedup of the Farallon plate, owing to additional entrained asthenospheric material. Such speedup is documented in studies of the Pacific plate circuit in early Paleogene (e.g., Wright et al., 2015), and is incorporated in the global plate motion reconstruction of Müller et al. (e.g., 2016). This information is shown in Fig. 4a, where we note a ~2 cm/yr increase of root mean square convergence velocity of Farallon and Kula plates relative to a moving hotspot reference frame around 55 Ma.

Since the relation between convergence velocity-change and $\Delta\bar{v}_{p,s}$ is not well known and beyond the scope of this study, we make a further simplification by fixing $\Delta\bar{v}_{p,s}$ as a constant within the vicinity of slab (~1000 km). To do so, we derive $\Delta P_{s,i}$ from a simple scaling argument:

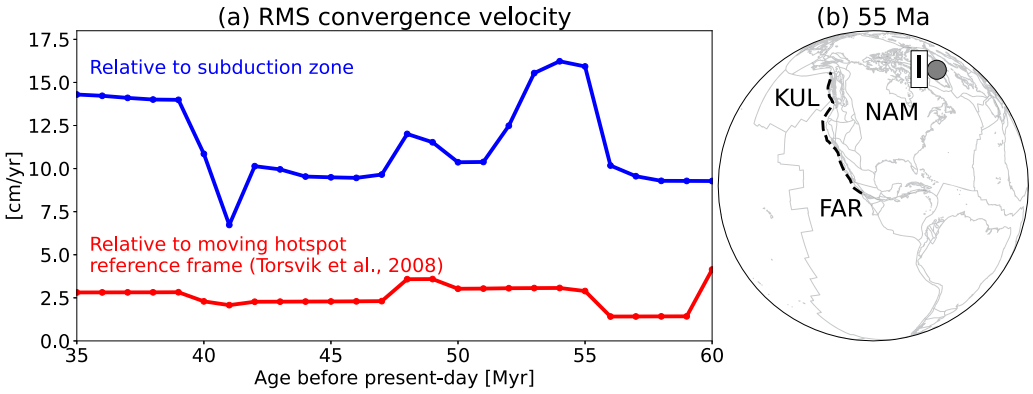

Fig. 4. (a): Root mean square (RMS) convergence velocity near western North America over a 1 Myr interval based on a global plate motion reconstruction (Müller et al., 2016). Blue and red lines show the RMS convergence relative to subduction zone and a global moving hotspot reference frame (Torsvik et al., 2008). Note an increase of RMS convergence near 55 Ma in both cases. (b). Plate configuration of western North America at 55 Ma. Dashed line indicates extracted convergent boundary based on the workflow developed by East et al. (2020). Grey circle is the present-day location of the Icelandic plume (I). FAR: Farallon. KUL: Kula. NAM: North America.

$$\Delta P_{s,i} \sim \frac{2\,|\,\bar{v}'_{p,s} - \bar{v}^0_{p,s}\,|}{H_a}\mu_a \tag{3}$$

where $|\,\bar{v}'_{p,s} - \bar{v}^0_{p,s}\,|$ is the norm of the velocity difference between a prescribed slab flow velocity $\bar{v}'_{p,s}$ and slab flow velocity beneath the subduction zone $\bar{v}^0_{p,s}$. Since we assume that the slab descends vertically, it is $\bar{v}^0_{p,s} = 0$ (i.e., $\bar{v}'_{p,s} - \bar{v}^0_{p,s} = \bar{v}'_{p,s}$). We note that the magnitude of $\Delta v_{p,s}$ is proportional to the number of sinks n (see Equation (2)). We therefore adjust n accordingly, so $\Delta v_{p,s}$ would approximately match $\bar{v}'_{p,s}$. In other words, $\Delta v_{p,s}$ is constrained deliberately by the input $\bar{v}'_{p,s}$.

Concerning our model parameterization, post-glacial rebound (PGR) studies (e.g., Paulson and Richards, 2009; Richards and Lenardic, 2018) have inferred a trade-off relation between asthenosphere viscosity and thickness: PGR models featuring a thick, stiff asthenosphere fit data as well as models featuring a thin, mobile channel. This trade-off has been parameterised by Paulson and Richards (2009) as $\mu_a/\mu_m \propto H_a^3$, where μ_m is the viscosity of the upper mantle underneath the asthenospheric channel. To address this non-uniqueness, we cast μ_a and μ_m as free parameters, ranging from $1\times10^{18} - 1\times10^{20}$ Pa·s and $5\times10^{20} - 4\times10^{21}$ Pa·s, respectively. We draw an ensemble of $\sim10^7$ (μ_a, μ_m) parameter pairs, and determine associated H_a based on inference from Paulson and Richards (2009). Among the (μ_a, μ_m, H_a) sets so obtained, we make a further selection by imposing also the Haskell constraint (Mitrovica, 1996), which states that the average upper mantle viscosity from the base of lithosphere to near 1400 km depth is $\sim$0.65–1.1 $\times\,10^{21}$ Pa · s. Fig. 5a shows the sampled (μ_a, μ_m, H_a) combinations that satisfy the trade-off relation inferred from PGR studies, where H_a is computed as the function of upper mantle viscosity contrast (i.e., μ_a/μ_m, see Paulson and Richards (2009)). Red bands represent boundaries where sampled parameter sets are compatible also with the Haskell constraint, having assumed a 100-km-thick lithosphere. After imposing the Haskell constraint, the ensemble reveals a limited range of plausible values of μ_m, which spans $\sim0.7 - 1.5\times10^{21}$ Pa · s, relative to the originally-sampled μ_m (i.e., $0.5 - 4\times10^{21}$ Pa · s).

To illustrate the sensitivity implied by this observationally-constrained parameterization, we select two (μ_a, H_a) sets: (1.4×10^{19} Pa · s, 100 km) and (7.5×10^{19} Pa · s, 200 km), and compute the associated North Atlantic asthenospheric flow in the early Paleogene. We choose these two parameter pairs, because their H_a range is in line with the tomographic inference of hot channelized asthenospheric material in the upper mantle (e.g., French et al., 2013; Celli et al., 2021). Figs. 5b - g illustrates the resulting flow fields. They depict the estimated Poiseuille-type flow at mid-asthenosphere depth due to the Icelandic plume, the Farallon slab and their combined effect. Overall, the predicted flow due to the Icelandic plume (Figs. 5b & e) features a radially outward pattern, where the velocity decays relative to the distance away from the plume center. The velocity magnitude differs slightly between two cases, owing to a different H_a^2/μ_a ratio (see Equation (1)). To estimate the flow pattern caused by the Farallon slab (Figs. 5c & f), we choose 2 cm/yr as the input $\Delta v'_{p,s}$, consistent with absolute convergence velocity change based on global plate motion reconstructions (Fig. 4). The slab flow field indicates a planar pattern beneath North America, where surrounding asthenospheric material is drawn towards the slab location. Figs. 5d & g shows the combined asthenospheric flow, which is the superposition of plume and slab flow fields. The resulting flow pattern illustrates a source-to-sink relation, where material sourced from Iceland is driven towards the Farallon slab, with a flow velocity of $\sim$5 cm/yr beneath North America. Note that the asthenospheric flow patterns between the two end-member parameter-sets are broadly similar. This relation indicates that our Poiseuille-type flow prediction is not significantly altered by the choice of (μ_a, H_a).

5. Torque variations upon plates in the North Atlantic region

The estimated asthenospheric flow exerts a shear-stress field at the base of the tectonic plates above, and thus results in an additional torque, or torque variation in the case of temporal changes of flow upon them. We compute such torque variation, and compare it with what is required to result in the kinematic changes indicated by reconstructions of the North Atlantic region. This approach allows us to quantitatively test whether the hypothesized asthenospheric process, which implies temporal flow changes, is a geodynamically-plausible candidate to explain the observed plate motion changes. The equations presented in the following are reprised from previous studies (e.g., Iaffaldano and Bunge, 2015; England and Molnar, 2022), and are reported here for completeness of information to the readership. The torque variation $\Delta\bar{M}$ required upon a plate in order to change its motion between two points in geologic time (t_1, t_2) is

$$\Delta\bar{M} = \int_A \frac{\mu_a}{H_a}\cdot\bar{r}\times[\bar{v}(\bar{r},t_1) - \bar{v}(\bar{r},t_2)]\,dA(\bar{r}) \tag{4}$$

where μ_a and H_a are asthenosphere viscosity and thickness. A is the plate basal area in spherical domain. $\bar{r}$ denotes the position vector of an infinitesimal plate basal area $dA(\bar{r})$. $\bar{v}(\bar{r},t)$ is the plate motion at position $\bar{r}$ and time t (see Iaffaldano and Bunge (2015) for detailed derivation). Since one can link the plate motion $\bar{v}(\bar{r},t)$ to the plate Euler vector $\bar{\omega}$ (i.e., $\bar{v}(\bar{r},t) = \bar{\omega}(t)\times\bar{r}$), Equation (4) can be rewritten as

$$\Delta\bar{M} = \int_A \frac{\mu_a}{H_a}\cdot[\bar{r}\times(\Delta\bar{\omega}\times\bar{r})]\,dA(\bar{r}) \tag{5}$$

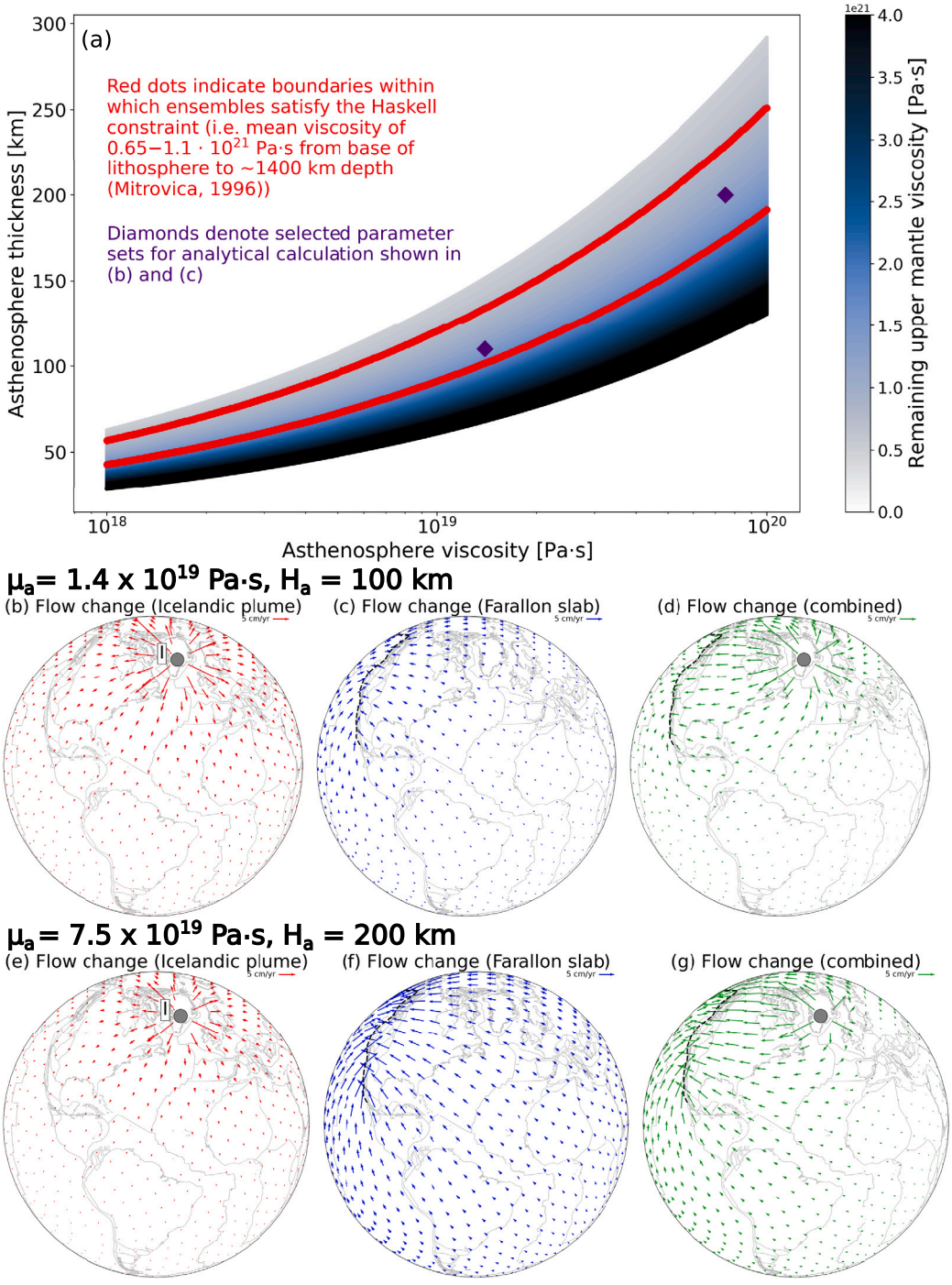

Fig. 5. (a). Ensemble of asthenosphere viscosity (μ_A), thickness (H_A) and remaining upper mantle viscosity (μ_M) based on the trade-off relation inferred from post glacial rebound (PGR) studies (e.g., Paulson and Richards, 2009; Richards and Lenardic, 2018). H_A is treated as a function of upper mantle viscosity contrast (i.e., $H_A = f(\mu_A/\mu_M)$, see text for details). Red circles indicate boundaries where ensemble satisfies the Haskell constraint (Mitrovica, 1996). Note the bounded parameter sets contain a limited range of μ_M between ~0.7–1.5 × 10^{21} Pa · s. Diamonds indicate two sets chosen for estimating the North Atlantic asthenospheric flow flux in Late Paleocene-early Eocene. Their H_A range is in agreement with the tomographic inference of hot channelized asthenospheric material in the upper mantle (e.g., French et al., 2013; Schaeffer and Lebedev, 2013). Panels (b)-(g) display the resulting flow fields associated with Icelandic plume (b & e), Farallon slab (c & f) and their combined effects (d & g). Note flow patterns are overall similar between two parameter sets, despite minor difference in velocity magnitude.

where $\Delta\bar{\omega}$ is the Euler-vector change between two stages, and is independent of $\bar{r}$. Thus Equation (5) can be written as a linear map (e.g., Martin de Blas and Iaffaldano, 2019; Espinoza and Iaffaldano, 2023)

$$\Delta\bar{M} = \mathbf{C}\Delta\bar{\omega} \tag{6}$$

where $\mathbf{C}$ is the plate-specific linear operator:

$$\mathbf{C} = \begin{bmatrix} c_{yy}+c_{zz} & -c_{xy} & -c_{xz} \\ -c_{yx} & c_{xx}+c_{zz} & -c_{yz} \\ -c_{zx} & -c_{zy} & c_{xx}+c_{yy} \end{bmatrix} \tag{7}$$

$$c_{ij} = \int_A \frac{\mu_a}{H_a} r_i r_j \, dA(\bar{r}) \tag{8}$$

Table 3
Entries of linear operator **C** from Equation (7) in this study.

Plate	C_{11} ($\times 10^{40}$ Pa · s · m^3)	C_{12}	C_{13}	C_{22}	C_{23}	C_{33}
NAM	24.86	2.72	-2.50	19.00	8.75	11.66
GRN	21.11	1.09	-7.84	23.77	2.51	3.77

The indices i, j denote Cartesian coordinates x, y and z. We draw 10^6 samples of each of the Euler vectors for the two stages considered, and use them to build ensembles of $\Delta\bar{\omega}$. We choose stages reported in Table 1, and resort to Equation (7) to map $\Delta\bar{\omega}$ samples into an ensemble of $\Delta\bar{M}$. The latter represents the minimum torque variation required to generate the North Atlantic plate kinematic change in late Paleocene-early Eocene. In order to compute **C**, we assign a thickness of 115 km and a viscosity of 2×10^{19} Pa · s to the model asthenosphere underneath NAM and GRN. This parameter pair represents the mean of the (H_a, μ_a) ensemble in Fig. 5a. Table 3 lists the resulting entries of **C** for each plate.

Next, we compute the torque variation associated with the change in asthenospheric Poiseuille-type flow ($\Delta\bar{M}_p$) over the time period from t_1 to t_2. We adopt the approach developed by Iaffaldano et al. (2018):

$$\Delta\bar{M}_p = \int_A \bar{r} \times \frac{2\mu_a}{H_a} \Delta\bar{v}_p(\bar{r}, t_1 - t_2)\, dA(\bar{r}) \tag{9}$$

where $\Delta\bar{v}_p(\bar{r}, t_1 - t_2)$ is the field describing the change of asthenospheric flow (Equations (1)-(3)). The factor 2 in Equation (9) relative to Equation (4) stems from the fact that the torque-variation estimate is based upon the force caused by underlying shear stress σ at the base of lithosphere. σ is obtained from a scaling relation in terms of the horizontal velocity gradient relative to an asthenosphere depth D (i.e., $\sigma = \mu_a \frac{\Delta v}{D}$). On the one hand, the parabolic nature of Poiseuille flow indicates that the maximum Δv occurs at the mid-asthenosphere (i.e., $D = 0.5H_a$; see Stotz et al. (2018); Vilacís et al. (2022) for schematic representation of Poiseuille/Couette flow). On the other hand, the Couette flow induced by the overlying plate motion has a linear envelope relative to asthenospheric depth, implying that the associated Δv reaches the maximum at its bottom (i.e., $D = H_a$).

Equations (5) & (9) also provide information about the orientation of the torque-variation exerted upon a plate. This information can be represented as a torque-variation pole, that is, the intersection of the torque-variation axis ($\Delta\bar{M}/|\Delta\bar{M}|$ and $\Delta\bar{M}_p/|\Delta\bar{M}_p|$) with Earth's surface. Figs. 6a-b show the comparison of poles obtained from the reconstructed plate-kinematic changes (black and grey circles; representing the mean of ensemble) as well as the estimated change in asthenospheric flow (colored circles). For the latter, we assign 700 m dynamic uplift as for the calculations in Figs. 5b-c to estimate the effect of the Icelandic plume-flow variation. For the flow induced by the Farallon slab descent, we consider three distinct cases with prescribed flow-velocity $\bar{v}'_{p,s}$ = 1, 2, and 4 cm/yr (see Equation (3)). Fig. 6a & b depict the torque-variation poles for NAM/EUA and GRN/EUA, respectively. Poles predicted by the Icelandic plume-flow change (red circle) are in close proximity with those obtained from kinematic reconstructions (black & gray circles). This proximity is prominent for GRN/EUA, where the predicted pole associated with plume-flow changes lies within the 99% confidence region of that associated with plate-motion changes. Together they indicate a good fit of torque-variation direction between reconstructed plate kinematics and asthenospheric Poiseuille-type flow induced by the Icelandic plume. Poles associated with predicted torque-variations start to deviate from those associated with reconstructed kinematic changes when one accounts for the effect of the Farallon slab descent.

Figs. 6c & d display the comparison of torque-variation magnitudes. Histograms are distributions of sampled torque variations based on reconstructed plate kinematics ($|\Delta\bar{M}|$). They indicate the minimum magnitude required in order to generate the inferred plate motion changes. Vertical solid lines are predictions based on estimated changes in asthenospheric flow ($|\Delta\bar{M}_p|$), while shaded regions represent the range obtained by assuming dynamic uplift due to the rising Icelandic plume between 500 and 900 m. This range is consistent with observational inferences from paleo-landscape studies (e.g., Jones et al., 2002; Hartley et al., 2011). In general, the distribution of $|\Delta\bar{M}|$ centers $\sim 2 \times 10^{25}$ and $\sim 3 \times 10^{24}$ Nm for NAM/EUA and GRN/EUA, respectively. The difference of nearly one order of magnitude arises from the different basal areas of NAM and GRN. We note that $|\Delta\bar{M}_p|$ associated with the Icelandic plume-flow change lies closely within the most recurrent 68% of estimated ensemble inferred from kinematic reconstructions. The addition of slab flow change, moreover, helps $|\Delta\bar{M}_p|$ to exceed the reconstructed $|\Delta\bar{M}|$, as expected. Together, they imply that the hypothesized asthenospheric flow processes could produce a torque variation that is i) sufficient and ii) oriented in the right direction in order to generate the reconstructed plate kinematic change.

6. Discussion

While being simplistic, the description of asthenospheric flow changes in terms of Couette/Poiseuille components (e.g., Phipps Morgan et al., 1995; Höink and Lenardic, 2008, 2010) provides an effective analytical framework to link rapid plate-motion variations with past dynamic topography signals. Though this inference is often expressed as torque balance upon plates (e.g., Iaffaldano et al., 2018), it requires knowledge of the history of horizontal and vertical plate motions that is preserved in different and independent geologic records. The history of horizontal plate motions during the past ~200 Myrs benefits from several decades of efforts in mapping the ocean-floor magnetization (e.g., Seton et al., 2014), and has received renewed attention over the past decade aimed at inferring plate kinematic changes at a temporal resolution of few Myrs (e.g., DeMets et al., 2015; Causer et al., 2021). Instead, inferences of past non-isostatic topographic changes, while relatively newer (e.g., Hoggard et al., 2021), can be put forth on the basis of extensive stratigraphic record available to the community.

The maps utilized here, which we compiled following the recently-developed approach of hiatus maps (e.g., Brown et al., 2022; Hayek et al., 2020; Vibe et al., 2018), aim to refine the North Atlantic vertical motion history with higher temporal resolution corresponding to geologic stages, and information of sediment type. One novel inference that can be drawn from our maps is that of episodes of terrestrial influx and end-of-hiatus signals, prominently in **Danian** and **Thanetian** (Fig. 3). This newly obtained information adds additional proxies to the Paleocene North Atlantic topography history, since previous maps, which featured resolution corresponding to geologic series, only depicted a single-phase hiatus in Europe at the same time (Hayek et al., 2020; Vibe et al., 2018). These refined signals, moreover, are in line with independent constraints on past vertical motion such as provenance studies (Morton et al., 2005), landscape analyses (e.g., Dam et al., 1998) and river profile inversion (e.g., de Quay and Roberts, 2023; Hartley et al., 2011). Together they support the notion of a multi-phase Paleocene topographic uplifts in the North Atlantic region. Such a notion is geodynamically plausible in the context of temporal variations of the Icelandic plume activity (e.g. Parnell-Turner et al., 2014), in which changes of active upwelling generate pulses of thermal anomalies through the plume conduit. These thermal pulses lead to episodic increases of Poiseuille-type flow in the low-viscosity asthenosphere, which in turn induce periodic surface uplifts.

On the other hand, the kinematic changes experienced by NAM and GRN occur in two different directions: southwest for the former, northwest for the latter (Fig. 2). This inference may suggest that two different geological processes are responsible for these different changes. However, under the assumption of the radially propagating Poiseuille-type flow flux associated with the Icelandic plume, the following observation is noteworthy: the paleo-position of GRN near late Paleocene-early

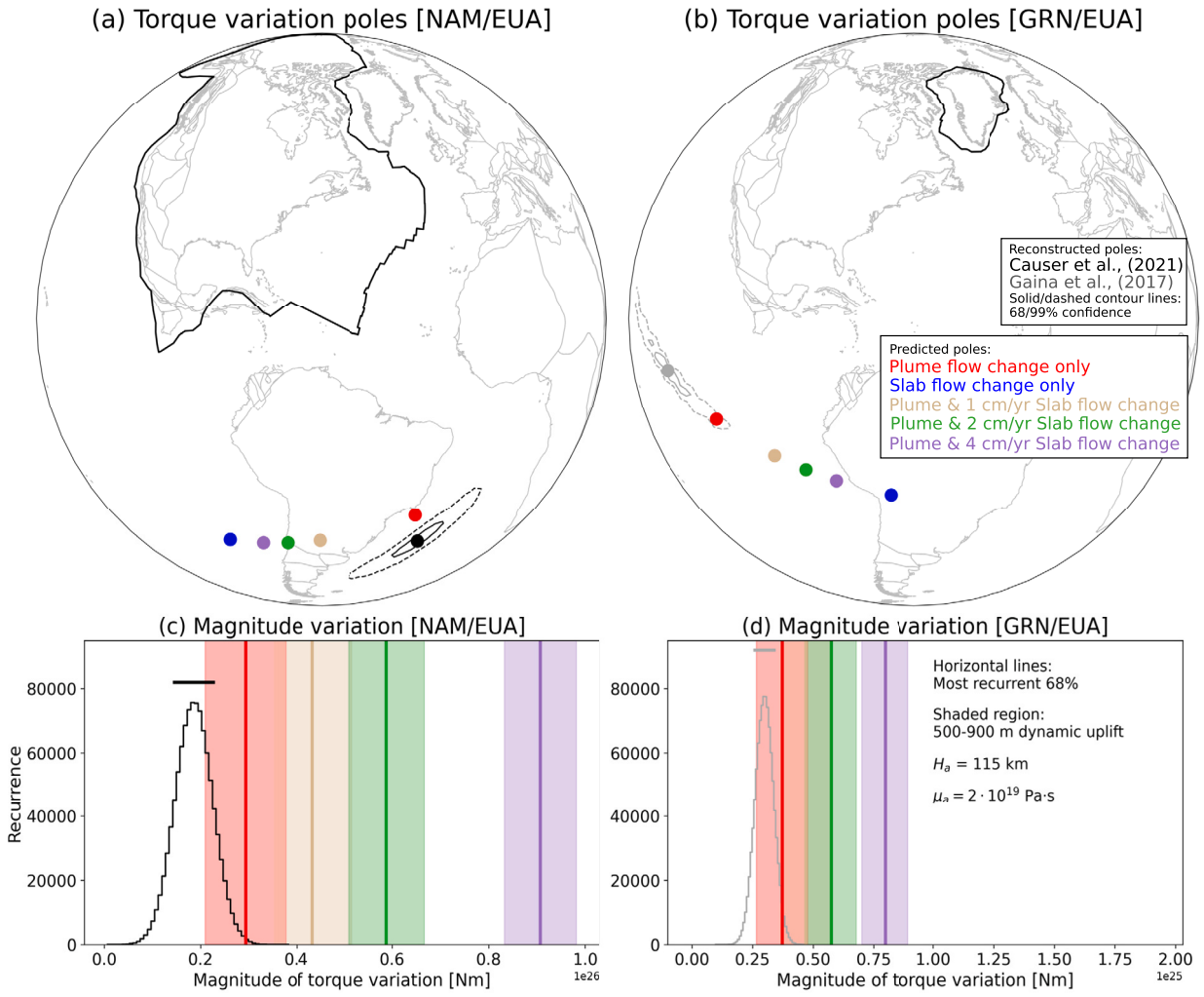

Fig. 6. (a) & (b): Comparison of torque variation poles for NAM/EUA and GRN/EUA, respectively. Black and grey circles indicate poles inferred from plate kinematic reconstructions. Solid/dashed contour lines are 68/99% confidence. Colored circles are poles predicted by analytical asthenosphere flow estimates. Here we choose a dynamic uplift of 700 m to compute the plume flow effect (see text for details). We assign a 115 km thick asthenosphere with a viscosity of 2×10^{19} Pa · s, since they represent the mean of parameter sets sampled in Fig. 5a. Note locations of predicted poles due to the plume flow change only are broadly compatible with reconstructed poles. (c) & (d): Associated toque magnitude variation. Histograms are distributions of sampled torque variation from plate kinematic reconstruction. Vertical lines and shaded regions are predicted torque variations based on asthenosphere flow estimates. Again note the close compatibility of torque-variation magnitude between kinematic inference and asthenospheric flow estimate related to the Icelandic plume flux only.

Eocene was such that the Icelandic plume was at its base in the southern region. This information implies that most of the asthenospheric radial flux coming from the Icelandic plume and in contact with the base of GRN had a strong component directed to the north. Meanwhile, the paleo-position of NAM was located west of the Icelandic plume, thus most of the Poiseuille-type flux in contact with the NAM base had a strong component directed to the west. These observational inferences make the notion of a single process responsible for both kinematic changes somewhat more plausible, at least to first-order. In addition, this divergent pattern of the kinematic changes experienced by NAM and GRN is consistent with the portion of outward Poiseuille-type flow direction produced by the plume (Figs. 5b & e) and sampled by the base of each plate.

Our hypothesis above is further supported by the torque analyses shown in Fig. 6. The latter reveals a proximity between torque-variation poles required for the reconstructed kinematic changes in the North Atlantic and provided by the asthenospheric flow-change hypothesized for the Icelandic plume. This inference suggests that the asthenospheric flow induced by the Icelandic plume alone is capable of generating a torque-variation direction that broadly agrees with the kinematic reconstruction. On the contrary, the asthenospheric flow effect due to the speedup of Farallon slab leads to a deviation of torque-variation poles away from the confidence region of those inferred from reconstructions. Such deviation implies that the slab is a less-likely candidate to explain the NAM and GRN plate kinematic changes. Apart from the directional information, the estimated magnitudes of torque-variations also indicate that the predicted range of plume-induced $\Delta \bar{M}_p$ is compatible with the most recurrent 68% of $\Delta \bar{M}$, required to generate the NAM and GRN kinematic changes (Figs. 6c & d). Moreover, this result holds under various (H_a, μ_a) combinations constrained by PGR data (Paulson and Richards, 2009; Richards and Lenardic, 2018) as well as the Haskell inference (Mitrovica, 1996) (Fig. 5a; see Supplementary Materials). Our inferred kinematic changes appear to occur after the proxy topographic uplifts deduced from stratigraphic record. This inference is in line with previous studies that correlate spreading-rate variations and proxy dynamic topography inferred from continental-scale hiatus maps in the Atlantic and Indo-Australia regions (Vibe et al. (2018); Vilacís et al. (2022)). Such time-lag is geodynamically plausible in terms of the time required for propagation of thermal plume pluses through its conduit into the low-viscosity, thin asthenosphere (e.g., Davies, 1999). Together these inferences support the notion that temporal variations of

the Icelandic plume activity have a significant role in influencing North Atlantic plate motion changes during the late Paleocene–early Eocene.

Nonetheless, some discrepancies exist between required and provided torque-variations (Figs. 6a & b). Such disagreement is particularly notable in the inference concerning NAM, where the predicted torque-variation pole lies outside the reconstructed 99% confidence region. On the one hand, such a discrepancy indicates the possibility that the asthenospheric flow change followed a slightly different pattern. On the other hand, we emphasize that the approach utilized here is a simplified one: we have, for instance, assumed a fixed EUA reference frame for the kinematic reconstruction. To this end, we note that our findings hold also in the case of torque-variations upon NAM tied to an absolute hotspot reference frame (see Supplementary Materials). Furthermore, we have assumed a constant asthenospheric thickness in our torque-variation predictions. In reality, the thickness of the low-viscosity asthenospheric channel appears irregular on global scale, particularly under continents, where thick cratonic roots have been imaged through seismic tomographic models (e.g., Celli et al., 2021). The presence of these roots would significantly reduce the asthenospheric thickness beneath continental regions, and alters locally the asthenospheric flow and thus the associated shear stress (e.g., Sleep, 1997). We also employ a Newtonian asthenospheric rheology, but there is alternative evidence pointing towards a non-Newtonian behavior of the upper mantle (e.g., Karato and Wu, 1993). The latter might lead to a more complex asthenospheric flow field in the form of "plug-flow", as indicated by recent geodynamic simulations (e.g., Semple and Lenardic, 2018). The formation of "plug-flow" means that it would no longer be possible to linearly superpose individual plume and slab Poiseuille flow components. Under an assumption of non-linear rheology, we would also expect a faster plume flow velocity due to a lower viscosity in the vicinity of the plume conduit, and hence a higher buoyancy flux (see Supplementary Materials for an estimate). While such rheology would in principle change the operator $\mathbf{C}$ (see Equation (7)), a recent study of plate torques that considers this non-linearity has found that it yields only minor variations of the torque estimates (England and Molnar, 2022). Furthermore, our modeled Icelandic plume flow is assumed to have a radially outward flow pattern in the asthenosphere. Nevertheless, there are growing constraints indicating a more complex flow pattern such as generation of "horizontal viscous fingers" (e.g. Schoonman et al., 2017).

In addition to the limitations naturally built into any quantitative model, we also point out some shortcomings of the observational inferences used here. The particular plate kinematic reconstructions feature a resolution of 5–10 Myrs that, while dictated by the coverage of ocean-floor magnetization maps available for the North Atlantic, is less that what available for other regions (~1 Myr resolution (e.g., DeMets et al., 2015; DeMets and Merkouriev, 2021)) during the Paleogene. Besides that, we resort to two independent studies to infer kinematics for NAM/EUA and GRN/EUA individually. Thus it is essential to test the resultant motion for NAM/GRN to ensure the closure of plate circuits (see Supplementary Materials).

The stage-resolution featured in unconformities maps reveal two major uplift phases in **Danian** and **Thanetian**. Paleo-landscape studies near North Sea have further resolved three successive topographic growth episodes since the **Thanetian** (e.g., de Quay and Roberts, 2023; Hartley et al., 2011). The inferred Thanetian uplift reflects an accumulation of these events, yet it lacks the sufficient temporal resolution to deduce them, therefore calling for additional refinements in the future. Whilst the maps used here provide proxies for the spatial extent of past dynamic topography, they lack associated magnitude information. The latter might be deduced by independent constraints on paleo-elevation, such as thermochronology (e.g., Ehlers and Farley, 2003), river profiles analysis (e.g., de Quay and Roberts, 2023; Hartley et al., 2011), and sedimentary compaction studies (e.g., Japsen, 2018). Furthermore, the geochronological dataset we resort to (Wilkinson et al., 2017) may also be subjected to non-systematic sampling bias.

7. Conclusion

In this study, we utilize publicly-available finite rotations to infer kinematic changes that occurred in the North Atlantic region during the early Cenozoic. Our analyses reveal a ~2-3 cm/yr velocity speedup of NAM and GRN in late Paleocene–early Eocene. These speedups coincide with episodes of proxy Paleocene topographic growth in the North Atlantic region, which are constrained by stage-resolution stratigraphic hiatus maps that we compiled as part of this study. These uplift events can be explained by the notion of transient behavior of Icelandic plume activity, and a subsequent increase of Poiseuille-type flow in the mechanically-weak asthenosphere. To quantitatively link these two independently-established surface signals, we estimate torque-variations i) required to explain the kinematic changes experienced by NAM and GRN, and ii) provided by temporal changes in the activity of the Icelandic plume flux, which we obtained via a parametrization of the consequent asthenospheric flow-change. We find that estimates of torque-variations are in close proximity with each other. Results, moreover, hold for different values of input parameters, including asthenospheric thickness & viscosity combinations, as well as when assuming an alternative reference frame for the kinematic reconstructions. Furthermore, our analyses account for the role of Poiseuille-type flow induced by the speedup of Farallon slab, evidenced in reconstructions of the Pacific kinematics. We note, however, that the inclusion of the latter effect tends to reduce the degree of fit between required and estimated torque-variations. In light of these results, we conclude that the Icelandic plume activity plays a primary role in controlling seemingly-unrelated signals of North Atlantic surface motions. The increase of Icelandic plume activity occurred in the early Paleogene is a geodynamically plausible candidate to simultaneously explain the uplift history of the surrounding regions and the speedups of NAM and GRN tectonic plates.

CRediT authorship contribution statement

Zhirui Ray Wang: Writing – original draft, Visualization, Validation, Software, Methodology, Investigation, Formal analysis, Conceptualization. **Giampiero Iaffaldano:** Writing – review & editing, Validation, Supervision, Methodology, Funding acquisition, Conceptualization. **John R. Hopper:** Writing – review & editing, Validation, Supervision, Funding acquisition, Data curation.

Declaration of competing interest

The authors declare that they have no known competing financial interests or personal relationships that could have appeared to influence the work reported in this paper.

Data availability

Finite-rotation parameters for NAM/EUA and GRN/EUA can be found in Causer et al. (2021) and Gaina et al. (2017), respectively. Moreover, their associated ocean-floor magnetic lineations can be found in Figure S1a-c in the Supplementary Material of Causer et al. (2021) (NAM/EUA) and Figure 3 in Gaina et al. (2017) (GRN/EUA). Stratigraphic data for inferring the North Atlantic vertical motion can be found in Hopper et al. (2014). Figures are plotted using the python package Matplotlib. Codes used in this study can be provided upon request.

Acknowledgements

We would like to thank two anonymous reviewers for their helpful and constructive comments, as well as to editor Alex Webb for carefully handling the manuscript. We would also like to thank Annabel Causer

and Graeme Eagles for valuable discussions about finite-rotation compilations in the North Atlantic region. This study is funded by Geocenter Danmark (Project number: 791572-5041).

Appendix A. Supplementary material

Supplementary material related to this article can be found online at https://doi.org/10.1016/j.epsl.2024.118831.

References

Anell, I., Thybo, H., Artemieva, I., 2009. Cenozoic uplift and subsidence in the North Atlantic region: geological evidence revisited. Tectonophysics 474, 78–105. https://doi.org/10.1016/j.tecto.2009.04.006.

Brown, H., Colli, L., Bunge, H.P., 2022. Asthenospheric flow through the Izanagi-Pacific slab window and its influence on dynamic topography and intraplate volcanism in East Asia. Front. Earth Sci. 10, 889907. https://doi.org/10.3389/feart.2022.889907.

Bunge, H.P., Richards, M.A., Baumgardner, J.R., 1996. Effect of depth-dependent viscosity on the planform of mantle convection. Nature 379, 436–438. https://doi.org/10.1038/379436a0.

Causer, A., Eagles, G., Pérez-Díaz, L., Adam, J., 2021. Cenozoic Relative Movements of Greenland and North America by Closure of the North Atlantic-Arctic Plate Circuit: the Labrador Sea, Davis Strait and Baffin Bay.

Celli, N.L., Lebedev, S., Schaeffer, A.J., Gaina, C., 2021. The tilted Iceland plume and its effect on the North Atlantic evolution and magmatism. Earth Planet. Sci. Lett. 569, 117048. https://doi.org/10.1016/j.epsl.2021.117048.

Chang, T., Stock, J., Molnar, P., 1990. The rotation group in plate tectonics and the representation of uncertainties of plate reconstructions. Geophys. J. Int. 101, 649–661. https://doi.org/10.1111/j.1365-246X.1990.tb05576.x.

Chase, C.G., 1978. Plate kinematics: the Americas, East Africa, and the rest of the world. Earth Planet. Sci. Lett. 37, 355–368. https://doi.org/10.1016/0012-821X(78)90051-1.

Cohen, K.M., Finney, S.C., Gibbard, P.L., Fan, J.X., 2013. The ICS international chronostratigraphic chart. Episodes, J. Int. Geosci. 36, 199–204. https://doi.org/10.18814/epiiugs/2013/v36i3/002.

Colli, L., Stotz, I., Bunge, H.P., Smethurst, M., Clark, S., Iaffaldano, G., Tassara, A., Guillocheau, F., Bianchi, M.C., 2014. Rapid south Atlantic spreading changes and coeval vertical motion in surrounding continents: evidence for temporal changes of pressure-driven upper mantle flow. Tectonics 33, 1304–1321. https://doi.org/10.1002/2014TC003612.

Courtillot, V., Davaille, A., Besse, J., Stock, J., 2003. Three distinct types of hotspots in the Earth's mantle. Earth Planet. Sci. Lett. 205, 295–308. https://doi.org/10.1016/S0012-821X(02)01048-8.

Dam, G., Larsen, M., Sønderholm, M., 1998. Sedimentary response to mantle plumes: implications from Paleocene onshore successions, West and East Greenland. Geology 26, 207–210. https://doi.org/10.1130/0091-7613(1998)026<0207:SRTMPI>2.3.CO;2.

Davies, G.F., 1999. Dynamic Earth: Plates, Plumes and Mantle Convection. Cambridge University Press.

Davies, G.F., Richards, M.A., 1992. Mantle convection. J. Geol. 100, 151–206. https://doi.org/10.1086/629582.

Davis, M.W., White, N.J., Priestley, K.F., Baptie, B.J., Tilmann, F.J., 2012. Crustal structure of the British Isles and its epeirogenic consequences. Geophys. J. Int. 190, 705–725. https://doi.org/10.1111/j.1365-246X.2012.05485.x.

DeMets, C., Iaffaldano, G., Merkouriev, S., 2015. High-resolution Neogene and quaternary estimates of Nubia-Eurasia-North America plate motion. Geophys. J. Int. 203, 416–427. https://doi.org/10.1093/gji/ggv277.

DeMets, C., Merkouriev, S., 2021. Detailed reconstructions of India–Somalia plate motion, 60 Ma to present: implications for Somalia plate absolute motion and India–Eurasia plate motion. Geophys. J. Int. 227, 1730–1767. https://doi.org/10.1093/gji/ggab295.

East, M., Müller, R.D., Williams, S., Zahirovic, S., Heine, C., 2020. Subduction history reveals Cretaceous slab superflux as a possible cause for the mid-Cretaceous plume pulse and superswell events. Gondwana Res. 79, 125–139. https://doi.org/10.1016/j.gr.2019.09.001.

Ehlers, T.A., Farley, K.A., 2003. Apatite (u–th)/he thermochronometry: methods and applications to problems in tectonic and surface processes. Earth Planet. Sci. Lett. 206, 1–14. https://doi.org/10.1016/s0012-821x(02)01069-5.

England, P., Molnar, P., 2022. Changes in plate motions caused by increases in gravitational potential energy of mountain belts. Geochem. Geophys. Geosyst. 23, e2022GC010389. https://doi.org/10.1029/2022GC010389.

Espinoza, V., Iaffaldano, G., 2023. Rapid absolute plate motion changes inferred from high-resolution relative spreading reconstructions: a case study focusing on the South America plate and its Atlantic/Pacific neighbors. Earth Planet. Sci. Lett. 604, 118009. https://doi.org/10.1016/j.epsl.2023.118009.

French, S., Lekic, V., Romanowicz, B., 2013. Waveform tomography reveals channeled flow at the base of the oceanic asthenosphere. Science 342, 227–230. https://doi.org/10.1126/science.1241514.

Friedrich, A.M., Bunge, H.P., Rieger, S.M., Colli, L., Ghelichkhan, S., Nerlich, R., 2018. Stratigraphic framework for the plume mode of mantle convection and the analysis of interregional unconformities on geological maps. Gondwana Res. 53, 159–188. https://doi.org/10.1016/j.gr.2017.06.003.

Gaina, C., Gernigon, L., Ball, P., 2009. Palaeocene–recent plate boundaries in the NE Atlantic and the formation of the Jan Mayen microcontinent. J. Geol. Soc. 166, 601–616. https://doi.org/10.1144/0016-76492008-112.

Gaina, C., Nasuti, A., Kimbell, G.S., Blischke, A., 2017. Break-up and Seafloor Spreading Domains in the NE Atlantic. Special Publications, vol. 447. Geological Society, London, pp. 393–417.

Gaina, C., Roest, W., Müller, R., 2002. Late Cretaceous–Cenozoic deformation of northeast Asia. Earth Planet. Sci. Lett. 197, 273–286. https://doi.org/10.1016/S0012-821X(02)00499-5.

Gordon, R.G., 1998. The plate tectonic approximation: plate nonrigidity, diffuse plate boundaries, and global plate reconstructions. Annu. Rev. Earth Planet. Sci. 26, 615–642.

Gregersen, U., Knutz, P., Nøhr-Hansen, H., Sheldon, E., Hopper, J., 2019. Tectonostratigraphy and evolution of the West Greenland continental margin. Bull. Geol. Soc. Denmark 67, 1–21. https://doi.org/10.37570/bgsd-2019-67-01".

Hager, B.H., Clayton, R.W., Richards, M.A., Comer, R.P., Dziewonski, A.M., 1985. Lower mantle heterogeneity, dynamic topography and the geoid. Nature 313, 541–545. https://doi.org/10.1038/313541a0.

Hager, B.H., O'Connell, R.J., 1981. A simple global model of plate dynamics and mantle convection. J. Geophys. Res., Solid Earth 86, 4843–4867. https://doi.org/10.1029/JB086iB06p04843.

Hartley, R.A., Roberts, G.G., White, N., Richardson, C., 2011. Transient convective uplift of an ancient buried landscape. Nat. Geosci. 4, 562–565. https://doi.org/10.1038/ngeo1191.

Hayek, J.N., Vilacís, B., Bunge, H.P., Friedrich, A.M., Carena, S., Vibe, Y., 2020. Continent-scale Hiatus maps for the Atlantic realm and Australia since the upper Jurassic and links to mantle flow induced dynamic topography. Proc. R. Soc. A 476, 20200390. https://doi.org/10.1098/rspa.2020.0390.

Hoggard, M., Austermann, J., Randel, C., Stephenson, S., 2021. Observational estimates of dynamic topography through space and time. Mantle convection and surface expressions, pp. 371–411.

Hoggard, M.J., Parnell-Turner, R., White, N., 2020. Hotspots and mantle plumes revisited: towards reconciling the mantle heat transfer discrepancy. Earth Planet. Sci. Lett. 542, 116317. https://doi.org/10.1016/j.epsl.2020.116317.

Höink, T., Lenardic, A., 2008. Three-dimensional mantle convection simulations with a low-viscosity asthenosphere and the relationship between heat flow and the horizontal length scale of convection. Geophys. Res. Lett. 35, L10304. https://doi.org/10.1029/2008gl033854.

Höink, T., Lenardic, A., 2010. Long wavelength convection, Poiseuille–Couette flow in the low-viscosity asthenosphere and the strength of plate margins. Geophys. J. Int. 180, 23–33. https://doi.org/10.1111/j.1365-246X.2009.04404.x.

Holbrook, W.S., Larsen, H., Korenaga, J., Dahl-Jensen, T., Reid, I., Kelemen, P., Hopper, J., Kent, G., Lizarralde, D., Bernstein, S., et al., 2001. Mantle thermal structure and active upwelling during continental breakup in the North Atlantic. Earth Planet. Sci. Lett. 190, 251–266. https://doi.org/10.1016/s0012-821x(01)00392-2.

Hopper, J.R., Funck, T., Stoker, M., Arting, U., Peron-Pinvidic, G., Doornenbal, H., Gaina, C., 2014. Tectonostratigraphic Atlas of the North-East Atlantic Region. Geological Survey of Denmark and Greenland.

Iaffaldano, G., Bunge, H.P., 2015. Rapid plate motion variations through geological time: observations serving geodynamic interpretation. Annu. Rev. Earth Planet. Sci. 43, 571–592. https://doi.org/10.1146/annurev-earth-060614-105117.

Iaffaldano, G., Davies, D.R., DeMets, C., 2018. Indian Ocean floor deformation induced by the reunion plume rather than the Tibetan Plateau. Nat. Geosci. 11, 362–366. https://doi.org/10.1038/s41561-018-0110-z.

Japsen, P., 2018. Sonic velocity of chalk, sandstone and marine shale controlled by effective stress: velocity-depth anomalies as a proxy for vertical movements. Gondwana Res. 53, 145–158. https://doi.org/10.1016/j.gr.2017.04.013.

Jones, S.M., White, N., Clarke, B.J., Rowley, E., Gallagher, K., 2002. Present and Past Influence of the Iceland Plume on Sedimentation. Special Publications, vol. 196. Geological Society, London, pp. 13–25.

Jones, S.M., White, N., Lovell, B., 2001. Cenozoic and Cretaceous Transient Uplift in the Porcupine Basin and Its Relationship to a Mantle Plume. Special Publications, vol. 188. Geological Society, London, pp. 345–360.

Karato, S.i., Wu, P., 1993. Rheology of the upper mantle: a synthesis. Science 260, 771–778. https://doi.org/10.1126/science.260.5109.771.

Martin de Blas, J., Iaffaldano, G., 2019. Using rigid microplate motions to detect the stress buildup preceding large earthquakes: a feasibility test based on synthetic models. J. Geophys. Res., Solid Earth 124, 13468–13485. https://doi.org/10.1029/2019JB018175.

McKenzie, D.P., Parker, R.L., 1967. The North Pacific: an example of tectonics on a sphere. Nature 216, 1276–1280. https://doi.org/10.1038/2161276a0.

Miall, A.D., 2016. The valuation of unconformities. Earth-Sci. Rev. 163, 22–71. https://doi.org/10.1016/j.earscirev.2016.09.011.

Minster, J.B., Jordan, T.H., 1978. Present-day plate motions. J. Geophys. Res., Solid Earth 83, 5331–5354. https://doi.org/10.1029/JB083iB11p05331.

Mitrovica, J.X., 1996. Haskell [1935] revisited. J. Geophys. Res., Solid Earth 101, 555–569. https://doi.org/10.1029/95JB03208.

Mitrovica, J.X., Beaumont, C., Jarvis, G., 1989. Tilting of continental interiors by the dynamical effects of subduction. Tectonics 8, 1079–1094. https://doi.org/10.1029/TC008i005p01079.

Morgan, W.J., 1968. Rises, trenches, great faults, and crustal blocks. J. Geophys. Res. 1896–1977 (73), 1959–1982. https://doi.org/10.1029/JB073i006p01959.

Morton, A., Whitham, A., Fanning, C., 2005. Provenance of late Cretaceous to Paleocene submarine fan sandstones in the Norwegian sea: integration of heavy mineral, mineral chemical and zircon age data. Sediment. Geol. 182, 3–28. https://doi.org/10.1016/j.sedgeo.2005.08.007.

Müller, R.D., Seton, M., Zahirovic, S., Williams, S.E., Matthews, K.J., Wright, N.M., Shephard, G.E., Maloney, K.T., Barnett-Moore, N., Hosseinpour, M., et al., 2016. Ocean basin evolution and global-scale plate reorganization events since Pangea breakup. Annu. Rev. Earth Planet. Sci. 44, 107–138. https://doi.org/10.1146/annurev-earth-060115-012211.

Ogg, J., 2020. Geomagnetic polarity time scale. In: Geologic Time Scale 2020. Elsevier, pp. 159–192.

Parnell-Turner, R., White, N., Henstock, T., Murton, B., Maclennan, J., Jones, S.M., 2014. A continuous 55-million-year record of transient mantle plume activity beneath Iceland. Nat. Geosci. 7, 914–919. https://doi.org/10.1038/ngeo2281.

Parnell-Turner, R., White, N., Henstock, T.J., Jones, S.M., Maclennan, J., Murton, B.J., 2017. Causes and consequences of diachronous v-shaped ridges in the North Atlantic Ocean. J. Geophys. Res., Solid Earth 122, 8675–8708. https://doi.org/10.1002/2017JB014225.

Parnell-Turner, R., White, N.J., McCave, I.N., Henstock, T.J., Murton, B., Jones, S.M., 2015. Architecture of North Atlantic contourite drifts modified by transient circulation of the Icelandic mantle plume. Geochem. Geophys. Geosyst. 16, 3414–3435. https://doi.org/10.1002/2015GC005947.

Paulson, A., Richards, M.A., 2009. On the resolution of radial viscosity structure in modelling long-wavelength postglacial rebound data. Geophys. J. Int. 179, 1516–1526. https://doi.org/10.1111/j.1365-246X.2009.04362.x.

Phipps Morgan, J., Morgan, W.J., Zhang, Y.S., Smith, W.H., 1995. Observational hints for a plume-fed, suboceanic asthenosphere and its role in mantle convection. J. Geophys. Res., Solid Earth 100, 12753–12767. https://doi.org/10.1029/95jb00041.

Poore, H.R., Samworth, R., White, N.J., Jones, S.M., McCave, I.N., 2006. Neogene overflow of Northern Component Water at the Greenland-Scotland Ridge. Geochemistry, Geophysics, Geosystems 7.

de Quay, G.S., Roberts, G.G., 2023. Geodynamic generation of a Paleocene–Eocene landscape buried beneath North Bressay, North Sea. J. Geol. Soc. 180, jgs2022–063. https://doi.org/10.1144/jgs2022-063.

Ribe, N.M., Tackley, P.J., Sanan, P., 2020. The strength of the Iceland plume: a geodynamical scaling approach. Earth Planet. Sci. Lett. 551, 116570. https://doi.org/10.1016/j.epsl.2020.116570.

Richards, F.D., Hoggard, M.J., White, N., Ghelichkhan, S., 2020. Quantifying the relationship between short-wavelength dynamic topography and thermomechanical structure of the upper mantle using calibrated parameterization of anelasticity. J. Geophys. Res., Solid Earth 125, e2019JB019062. https://doi.org/10.1029/2019JB019062.

Richards, M.A., Lenardic, A., 2018. The Cathles parameter (Ct): a geodynamic definition of the asthenosphere and implications for the nature of plate tectonics. Geochem. Geophys. Geosyst. 19, 4858–4875. https://doi.org/10.1029/2018GC007664.

Rudge, J.F., Champion, M.E.S., White, N., McKenzie, D., Lovell, B., 2008. A plume model of transient diachronous uplift at the Earth's surface. Earth Planet. Sci. Lett. 267, 146–160. https://doi.org/10.1016/j.epsl.2007.11.040.

Schaeffer, A., Lebedev, S., 2013. Global shear speed structure of the upper mantle and transition zone. Geophys. J. Int. 194, 417–449. https://doi.org/10.1093/gji/ggt095.

Schoonman, C., White, N., Pritchard, D., 2017. Radial viscous fingering of hot asthenosphere within the Icelandic plume beneath the North Atlantic Ocean. Earth Planet. Sci. Lett. 468, 51–61. https://doi.org/10.1016/j.epsl.2017.03.036.

Semple, A.G., Lenardic, A., 2018. Plug flow in the Earth's asthenosphere. Earth Planet. Sci. Lett. 496, 29–36. https://doi.org/10.1016/j.epsl.2018.05.030.

Seton, M., Whittaker, J.M., Wessel, P., Müller, R.D., DeMets, C., Merkouriev, S., Cande, S., Gaina, C., Eagles, G., Granot, R., Stock, J., Wright, N., Williams, S.E., 2014. Community infrastructure and repository for marine magnetic identifications. Geochem. Geophys. Geosyst. 15, 1629–1641. https://doi.org/10.1002/2013GC005176.

Sleep, N.H., 1997. Lateral flow and ponding of starting plume material. J. Geophys. Res., Solid Earth 102, 10001–10012. https://doi.org/10.1029/97JB00551.

Stotz, I.L., Iaffaldano, G., Davies, D.R., 2018. Pressure-driven Poiseuille flow: a major component of the torque-balance governing Pacific plate motion. Geophys. Res. Lett. 45, 117–125. https://doi.org/10.1002/2017GL075697.

Torsvik, T.H., Müller, R.D., Van der Voo, R., Steinberger, B., Gaina, C., 2008. Global plate motion frames: toward a unified model. Rev. Geophys. 46. https://doi.org/10.1029/2007RG000227.

Vibe, Y., Friedrich, A.M., Bunge, H.P., Clark, S., 2018. Correlations of oceanic spreading rates and hiatus surface area in the North Atlantic realm. Lithosphere 10, 677–684. https://doi.org/10.1130/L736.1.

Vilacís, B., Hayek, J.N., Stotz, I.L., Bunge, H.P., Friedrich, A.M., Carena, S., Clark, S., 2022. Evidence for active upper mantle flow in the Atlantic and Indo-Australian realms since the upper Jurassic from hiatus maps and spreading rate changes. Proc. R. Soc. A 478, 20210764. https://doi.org/10.1098/rspa.2021.0764.

Wang, Z.R., Stotz, I.L., Bunge, H.P., Vilacís, B., Hayek, J.N., Ghelichkhan, S., Lebedev, S., 2023. Cenozoic upper mantle flow history of the Atlantic realm based on Couette/Poiseuille models: towards paleo-mantle-flowgraphy. Phys. Earth Planet. Inter. 340, 107045. https://doi.org/10.1016/j.pepi.2023.107045.

White, N., Lovell, B., 1997. Measuring the pulse of a plume with the sedimentary record. Nature 387, 888–891. https://doi.org/10.1038/43151.

White, R.S., 1997. Rift–plume interaction in the North Atlantic. Philos. Trans. R. Soc. Lond., Ser. A, Math. Phys. Eng. Sci. 355, 319–339. https://doi.org/10.1098/rsta.1997.0011.

Wilkinson, C.M., Ganerød, M., Hendriks, B.W., Eide, E.A., 2017. Compilation and Appraisal of Geochronological Data from the North Atlantic Igneous Province (NAIP). Special Publications, vol. 447. Geological Society, London, pp. 69–103.

Wright, N.M., Müller, R.D., Seton, M., Williams, S.E., 2015. Revision of Paleogene plate motions in the Pacific and implications for the Hawaiian-emperor bend. Geology 43, 455–458. https://doi.org/10.1130/G36303.1.